Novel Flyweight Three-Dimensional Self-Assembled Graphene Oxide/Octa(Aminophenyl) Polyhedral Oligomeric Silsesquioxane Hybrid Aerogels

Jangi, Abolfal; Rezaei, Mostafa*+; Talebi, Saeid*+
Faculty of Polymer Engineering, Sahand University of Technology, Tabriz, I.R. IRAN

Haghgoo, Majid
Space Transportation Research Institute, Iranian Space Research Center, Tehran, I.R. IRAN

ABSTRACT: *Herein, flyweight organic-inorganic hybrid scaffolds were fabricated by self-assembly and reduction of graphene oxide via covalent reaction of octa(aminophenyl) polyhedral oligomeric silsesquioxane with graphene oxide. Octa(aminophenyl) polyhedral oligomeric silsesquioxane created a decorative coating on the graphene oxide surface. It acts as a nano-crosslinker, especially on the overlapped-zone of graphene oxide platelets to bind them close-fitting. The resulting hybrid hydrogel was transformed into aerogel by the solvent exchange process with liquid carbon dioxide, followed by liquid carbon dioxide supercritical drying. Different concentrations of graphene oxide and octa(aminophenyl) polyhedral oligomeric silsesquioxane were prepared and the structure-property relationship of obtained aerogels is elucidated. Bulk density and porosity of the aerogels are located between the super-low values of 2.7 to 5.9 mg/cm^3 and beyond 99.5 %, respectively. According to the adsorption-desorption isotherms of BET-technique, the surface area of obtained aerogels was in between 250 to 713 m$^{2/}$g. The findings remark the potential application of obtained aerogels in the production of supercapacitors, lithium-ion batteries, solar cells, etc. in energy storage and conversion devices, electrode materials, sensors, gas/oil/dye adsorbents, and high-temperature insulators in the aerospace industry.*

KEYWORDS: *Flyweight organic-inorganic aerogel; Graphene oxide hybrid aerogel; 3D porous architecture; Supercritical drying; Energy storage and conversion devices*.

INTRODUCTION

In the shadow of the quick growth of industry and strongly request for high-performance materials, the indispensability for research in the field of material science is sensed more than ever. Graphene is a nanomaterial allotrope of carbon as a two-dimensional crystal, a single carbon atom thick, and one of the most appealing materials [1].

** To whom correspondence should be addressed.*
+ E-mail: rezaei@sut.ac.ir & talebi@sut.ac.ir
1021-9986/2021/3/743-757 15/$/6.05

Since its emersion in 2004, thanks to its fantastic properties, graphene has been in the limelight of experts in the previous decade. Outstanding mechanical properties (tensile strength and elastic modulus of about 130 GPa and 1.1 TPa, respectively) [2], brilliant charge-carrier mobility [3], worthy durability versus chemical materials, and extreme thermal conductivity [4] are some striking properties of this amazing material [5, 6].

Graphene Aerogels (GAs) are 3D framework supermaterials [7], which are made of graphene and have been used in an extensive scope of scientific and industrial applications [8, 9]. Owing to their prominent properties such as ultra-lightweight [10], enormous theoretical specific surface area of 2600 m^2/g, high porosity [11, 12], GAs show an inordinate potential going to use in energy storage and conversion material and devices, namely, SuperCapacitors (SCs), Lithium-Ion Batteries (LIBs), solar cells, etc. in the electronics and energy industries [13-16], electrode materials [17, 18], gas/oil/dye adsorbents [19-23], catalyst supports [24], and thermal insulators at high temperatures in the aerospace industry [25-27].

In practice, as a result of its heavy functionality and subsequently, high dispersibility in common solvents [28], graphene oxide (GO), a kind of graphene derivative, is a fitting starting material to assemble three-dimensional graphene frameworks [29, 30]. The oxygen-containing functional groups of GO are capable of chemically react with diverse constituents. Therefore, GO is extremely beneficial as starting unit to synthesize numerous graphene-based aerogels. [5, 6, 31].

A good deal of investigation has been performed to enrich deficiency of monolithic lightweight porous carbon materials (i.e. graphene aerogels), involving low physicochemical property, extra low mechanical property, inferior thermal stability, and fair electrical property. Between them, synthesizing doped or coupled hybrid aerogel [32-35], making composite aerogel [34, 36, 37], and using a physical or chemical binding agent [15, 33, 34] have been well investigated.

Alternatively, octa(aminophenyl) polyhedral oligomeric silsesquioxane (OapPOSS), an organic-inorganic silica supermolecule, with its unique core-shell molecular arrangement, has grabbed substantial attention because of its exciting physicochemical characteristics. They enjoy features such as superhydrophobicity, great mechanical properties, high thermal stability, worthy oxidation resistance, and good flame retardancy [38-40]. It surrounded by hyperbranched organic aminophenyl substituents at eight vertices. These octa-reaction sites can be used for further functionalization, making OapPOSS a perfect modification agent [38, 41].

Obviously, the novel nanostructured hybrid that involves carbon- and POSS-based nanomaterials (both solid matter and aerogel), may possibly merge the properties of both starting building block, lead to improving some inferior properties of ingredients.

In several kinds of research, POSS-modified GO was synthesized with the aim of improving the specifications of resulting hybrid nanocomposite material. *Liao* and *coworkers* [42] were used surface-functionalized graphene oxide platelets with octa(aminophenyl) polyhedral oligomeric silsesquioxane as a porous nanofiller to the polyimide matrix with super-strong mechanical characteristics and minor dielectric constant. *Hu et al.* [43] were successfully prepared octa(aminopropyl) polyhedral oligomeric silsesquioxane functionalized graphene oxide. This nanomaterial was incorporated into waterborne polyurethane to increase mechanical properties, thermal resistance, and hydrophobicity of the related nanocomposites. Likewise, in another research [44], the coupling of amino-POSS with graphene oxide was reported, as a nanofiller with superhydrophobic properties (a contact angle of ~157°) and high thermal properties. Recently, *Zong et al.* [45] prepared a novel hybrid material of GO/aminopropylisobutyl polyhedral oligomeric silsesquioxane to increase thermal conductivity and electrical insulating features of epoxy composite materials. Very recently, *Namvari et al.* [46] developed cross-linked rGO–POSS hybrid material through click reaction, with high hydrophobicity and well solubility in various organic solvents, used as filler for fabricating polydimethylsiloxane nanocomposites.

In this research, for the first time, we synthesized ultra-lightweight octa(aminophenyl) polyhedral oligomeric silsesquioxane/graphene oxide monolith aerogel with high porosity and high surface area. It is believed, in addition that OapPOSS molecules decorate the surface of GO platelets; they could link graphene in the conjointment of nanosheets resulting in a novel nanostructured hybrid aerogel material. The microstructure and physicochemical properties of the intermediate and resulting aerogels were investigated by Fourier-Transform InfraRed (FT-IR), UV-Vis, Raman scattering,

X-Ray Riffraction (XRD), Brunauer–Emmett–Teller (BET), and Feld Emission Scanning Electron Microscopy (FESEM), and the details of the structure-property relationship were discussed for the resultant hybrid aerogels.

EXPERIMENTAL SECTION

Materials

Graphene nanosheets were provided by US Research Nanomateials, Inc. Sulfuric acid 98% (H_2SO_4), potassium permanganate ($KMnO_4$), sodium nitrate salt ($NaNO_3$), hydrogen peroxide solution 30% (H_2O_2), hydrochloric acid fuming 37% (HCl), tetrahydrofuran (THF) and acetone were all of reagent grade and supplied by Merck Co. Octa(aminophenyl) polyhedral oligomeric silsesquioxane (OapPOSS) was purchased from Mayaterials, Inc (Michigan, USA). All chemical materials were used as received.

Synthesis of Graphene Oxide (GO)

Modified Hummers' technique was utilized to synthesize GO [47]. First, graphene nanosheets powder (5 g) was poured into a 500 mL two-necked reactor containing H_2SO_4 (120 mL) while mixing at room temperature. Then, $NaNO_3$ salt (2.5 g) was added to the reactor and the mixture was agitated at room temperature for 2 hours. Then, the reaction system was placed in an ice bath and under intensive stirring and simultaneously monitoring the temperature below 13 °C, $KMnO_4$ (15 g) was gradually added into the reactor within 30 minutes. The reaction setup was subsequently located in a bath and the temperature was set at 35 °C. The viscosity of the reaction mixture increased over time within 24 hours and a viscous paste was finally obtained. While the temperature was controlled below 60 °C, deionized water (150 mL) was slowly added to the viscous pasty mixture. Stirring of the resulting suspension was continued for extra 24 hours. The prepared suspension was added slowly into a 5-liter beaker, containing distilled water (2 liters) and H_2O_2 (50 mL), while the solution was stirring. Since then, the mixture color changed from brownish to yellowish. After allowing the suspension to be precipitated, it was isolated from the supernatant acid by the decanting technique. To remove the metal ions, the resulting solid material was washed with 5% HCl (1 liter), and the supernatant was then decanted away from sediment. The remaining solid material was then multiple-washed with distilled water, and each time to precipitate suspended solid materials, the centrifugation technique was applied (9000 rpm). To remove any trapped water, the resulting solid was vacuum-dried overnight at 60 °C. To exfoliate the graphene oxide nanoplatelets, the attained powder was finally sonicated (180 W, a 0.5 cycle for 90 minutes) in an ice bath below 10 °C.

Preparation of hybrid GO-OapPOSS aerogels (GOPOS aerogels)

A simple and straightforward method was used to make organic-inorganic hybrid GO-OapPOSS aerogels (GOPOS aerogels). First, as-synthesized GO was transferred into the reaction media, namely H_2O/THF, in a beaker and was then dispersed by ultrasonication technique. Whereas the suspended GO stirring, OapPOSS was added to the system at room temperature. Resulting homogeneous suspension was poured into a container and transferred to an autoclave reactor (80 °C, 24 hours) in order to obtain Graphene oxide/OapPOSS gel. Finally, the solvent exchange method was carried out, followed by CO_2 supercritical drying to obtain corresponding aerogels (See Supplementary data S1, S2, and S3).

Characterization methods

Skeletal density (ρ_s) of the resultant aerogels was measured by a helium pycnometer from Micromeritics (model Accupyc 1330). The bulk density (ρ_b) of the aerogels was calculated through dividing the sample weight (m_s) by volume of the same samples (V_s, determined by a 3D optical scanner). A Nicolet Fourier transform infrared/visible spectrometer (model 6700), from Thermo Scientific was used to study FT-IR spectra of the raw materials functional groups as well as to follow the formed or disappeared covalent bonds during the reaction. Fifteen scans were gathered with a spectral resolution of 1 cm^{-1}. Less enough concentration of specimen on KBr disc was used to confirm the Beer-Lambert rule. Raman spectra were recorded from 200 to 4000 cm^{-1} on an Almega Thermo Nicolet Dispersive Raman Spectrometer (Horiba Jobin Yvon Instruments, France). 32 scans with a spectral resolution of 4 cm^{-1} were accumulated using a 532 nm of a 100 mW Nd: YLF laser. A UV/Vis high-performance double beam spectrophotometer (model T80+) from PG Instruments Ltd, with pre-aligned tungsten and deuterium lamps, a spectral range

of 190-1100 nm, and wavelength accuracy of ±0.3 nm was used to record UV/Vis absorption spectra of the samples. For all specimens, a clean quartz slide was applied as the reference. To explore how the structures of intermediate and final samples were transformed, the X-Ray Diffraction (XRD) measurements were conducted by an X'Pert MPD model diffractometer from Philips with an area detector working under a voltage of 40 kV and a current of 40 mA employing Co as the source (λ= 1.78897 Å). The microstructures, elemental mapping and quantitative analysis of the aerogels were characterized using a TESCAN MIRA3 XMU VP- Field Emission Scanning Electron Mmicroscope (FESEM) after sputter coating the aerogels with gold. Porous characteristics of the resultant aerogels such as specific surface area, average pore size, BJH pore size distribution, and pore volume were measured by the nitrogen gas adsorption-desorption technique with a BELSORP-mini II instrument, according to Brunauer-Emmett-Teller theory. Prior to characterization, the aerogels were vacuum-degassed at 80 °C for 8 hours to eliminate water, CO_2, air and other physically adsorbed species from the pores of aerogels.

RESULTS AND DISCUSSION

Herein, it was aimed to prepare organic-inorganic hybrid monolith aerogel with high porosity and good physicochemical property, through simultaneous self-assembling and reduction of GO via covalent coupling of GO with OapPOSS. It is expected that the OapPOSS molecule could be bonded to GO nanoplatelet in two ways; (i) through the crosslinking of GO platelets *via* nucleophilic attack of amine groups of OapPOSS on oxygen-containing groups of overlapped-zone of GO nanosheets, and (ii) through covalently grafting of OapPOSS molecule on GO sheet via amine branches of OapPOSS and far-conjointment oxygen-functionalized groups of GO, resulting to surface decorating of GO platelets. A schematic diagram of the procedure to synthesize the GOPOS hybrid aerogels is illustrated in Fig. 1.

Several compositions of GO and OapPOSS (Table 1) were formulated to explore the influence of the ingredients on morphology and physical characteristics of resultant aerogels. The numbers in the sample code denote the GO in the formulation in percentage. The raw materials concentration varies from 0.4 to 3.6 mg/cm^3, whereas the total solid content was kept constant at 4 mg/cm^3.

The preparation process and the GOPOS hybrid aerogel monoliths product are shown in Fig. 2. After the reactants were ultrasonicated in H_2O/THF media (Fig. 2a), a homogeneous suspension was obtained (Fig. 2b). Then all vials were kept at a fixed temperature for a certain time in an autoclave reactor (Fig. 2c and d). Accordingly, GOPOS hybrid gels, floating GOPOS hybrid gels on the top of the solvent, were obtained (Fig. 2e). To preserve 3D porous nanostructure of the GOPOS gels the solvent exchange process was performed (Fig. 2f and g). Finally, by CO_2 supercritical drying (Fig. 2h) the desired aerogels were achieved. Pictures of ultra-lightweight GOPOS hybrid aerogels monolith, placed on top of a Hordeum marinum and Taraxacum kok-saghyz, are shown in Fig. 2i and j, respectively.

Chemical characterization of synthesized GOPOS aerogels

The Fourier Transform InfraRed (FT-IR) spectroscopic technique was employed to determine GO, OapPOSS, and resulting GOPOS aerogels functional groups and likewise, to explore chemical linkages that are constituted or vanished during the coinciding reaction and gel creation (Fig. 3).

As illustrated in Fig. 3, the absorption bands of GO are found at nearly 3000 ~ 3700 cm^{-1}, 1720 cm^{-1}, 1550 ~ 1650 cm^{-1}, and 1050 cm^{-1} which are ascribed to stretching vibration of O-H hydroxyl group with contribution from COOH and H_2O (i.e., C–OH), C=O carboxylic group, in-plane stretching C=C, and the -C-O- epoxy rings stretching mode, respectively [48, 49]. The absorption peaks of OapPOSS which are located at around 3378 cm^{-1}, 1596 cm^{-1}, 1114 cm^{-1}, 836 cm^{-1}, and 759 cm^{-1} are allotted to the N-H stretching vibration of –NH_2 aromatic group, the stretching vibration of –NH_2 group, vibrational feature of Si-O-Si linkage, particular vibrational specification of the Si-O-Si cage scaffold, and Si-C bind bending vibration in the Si-phenyl ring, respectively [50].

The absorption bands of these groups undergo a major decrease after incorporation of OapPOSS into the GOPOS aerogels. Particularly, the -C-O- stretching vibration of epoxy group at 1065 cm^{-1} was completely disappeared clarifying ring opening reaction. The band intensity of the C=O carboxylic group of GO at 1720 cm^{-1} was almost remained intact and slightly shifted towards a lower frequency of 1710 cm^{-1} revealing less chance of formation of C=O amide group [51]. The newly emerged peak

Table 1: Different compositions of GOPOS aerogels.

Parameter	Quantity				
Sample code	GOPOS10	GOPOS30	GOPOS50	GOPOS70	GOPOS90
GO [mg]	10	30	50	70	90
OapPOSS [mg]	90	70	50	30	10
THF/H_2O volume [mL]	25				
THF/H_2O volume ratio	1:1				

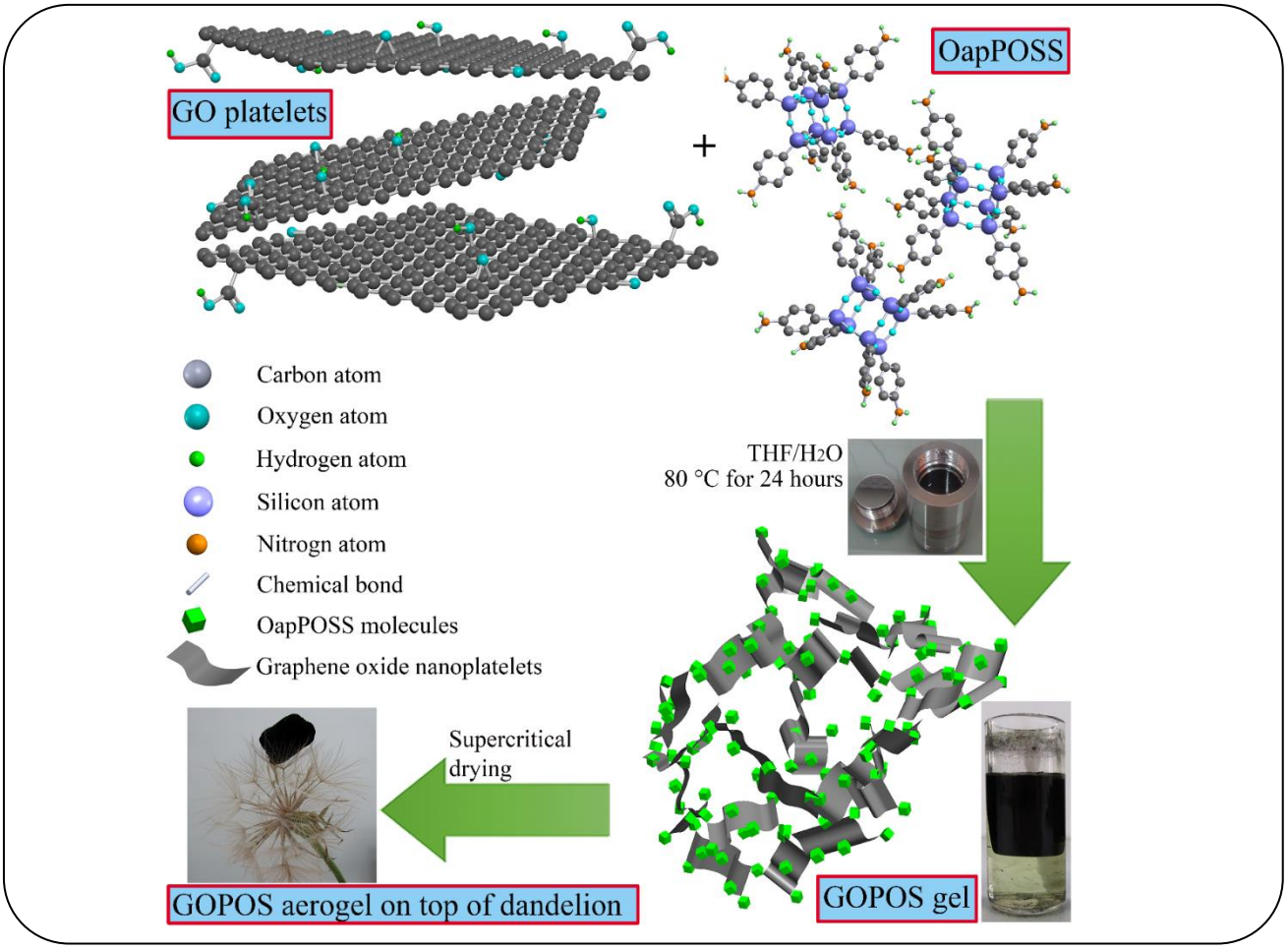

Fig. 1: A Schematic diagram of the preparation process of GOPOS aerogels.

at 1349 cm^{-1} and the peak located at nearby 1589 cm^{-1}, in all GOPOS aerogels, is attributed to fresh formed -C-N- bond and in-plane bending of N-H bond (existing in probably non-reacted $–NH_2$ groups of OapPOSS and newly formed amine or possibly amide bonds), respectively, implying OapPOSS was successfully merged into the GOPOS aerogels. The characteristic peaks relevant to the Si-O-Si and Si-C groups is another evidence that OapPOSS was efficiently introduced in GOPOS aerogels [50, 52]. Supplementary information concerning FT-IR results of all specimens is included in the Supporting Fig. S4.

UV-Vis spectroscopy, as depicted in Fig. 4, was performed in order to verify whether the OapPOSS molecules are presented in GOPOS aerogels.

Inspection of UV-Vis absorption spectrum of GO illustrates two wide bands at around 224 and 327 nm

Fig. 2: Preparation procedure of GOPOS aerogels: ultrasonication process to disperse reagents in H2O/THF solvent (a), dispersed reactants in solvent media; left to right: GOPOS90, GOPOS70, GOPOS50, GOPOS30, GOPOS10 (b), reaction autoclave (c) and (d), assembled GOPOS gels; left to right: GOPOS90, GOPOS70, GOPOS50, GOPOS30, GOPOS10 (e), solvent exchange process (f) and (g), supercritical CO2 dryer to convert gels to aerogels (h), digital photographs of flyweight GOPOS aerogels placed on top of a Hordeum marinum (i) and Taraxacum kok-saghyz(j).

with a shoulder at nearby 302 nm which can be related to the π-π^* electron transition of sp^2 C=C binds, and n- π^* electron transitions of C=O links, respectively [28, 44]. The absorption spectrum of OapPOSS demonstrates no absorption peak behind of 342 nm, instead of two distinct bands at around 247 and 305 nm can be clearly observed. The prepared GOPOS aerogels demonstrate two absorptions peaks at nearby 251 and 308 nm, which could be the equivalent OapPOSS bands at 247 and 305 nm with a red-shift of 4 and 3 nm, respectively. The characteristic absorption peak of GOPOS aerogels at 308 nm, was extended to the wavelength of over 342 nm (See supporting Fig. S5), confirming the existence of OapPOSS in the GOPOS aerogel materials. In fact, the covalent bond of $-NH_2$ amine groups of OapPOSS and the oxygen-functionalized groups of GO has enhanced the optical absorption by increasing the interaction length of light, leading to the ease of electron excitation [44, 52].

The structural and electronic properties of pristine materials and prepared aerogels, involving disordered and abnormal structures were examined by Raman spectrum given in Fig. 5.

According to this figure, two prominent bands for GO are located at approximately 1348 cm^{-1} (D band) and 1595 cm^{-1} (G band),

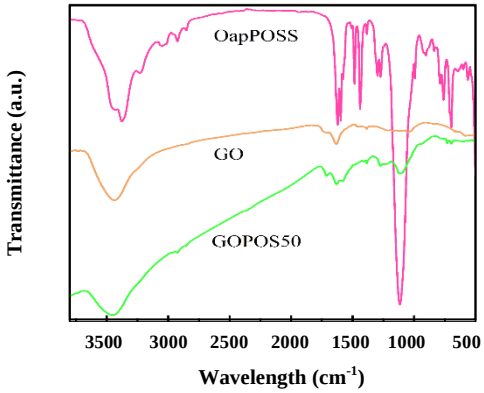

Fig. 3: FT-IR spectra of GO, OapPOSS, and typically presented GOPOS50 aerogel.

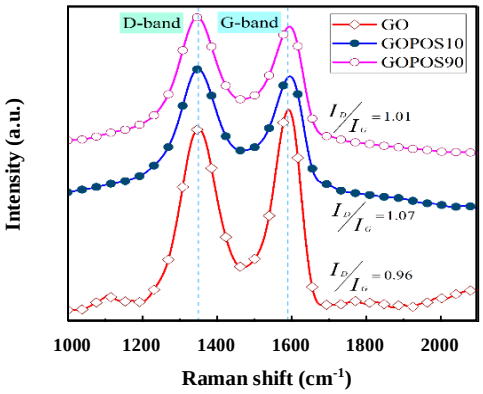

Fig. 5: Raman spectra of graphene, GO, typically demonstrated GOPOS10 and GOPOS90 aerogels.

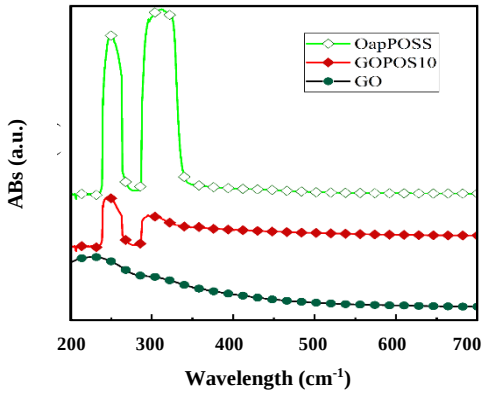

Fig. 4: UV-vis spectra of GO, OapPOSS, and typically presented GOPOS10 aerogel.

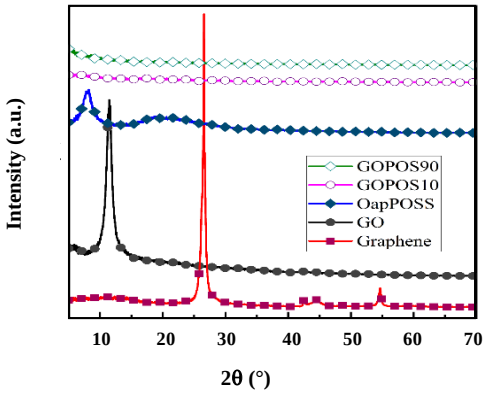

Fig. 6: XRD patterns of graphene, GO, OapPOSS, typically illustrated GOPOS10 and GOPOS90 aerogels.

1595 cm^{-1} (G band), attributed to the K point phonons of A_{1g} symmetry mode due to the structural sp^3-hybridized carbon atom imperfections and the zone center phonons of E_{2g} symmetry mode arises from lattice deflection in sp^2-hybridized carbon atoms, respectively [43]. In GOPOS aerogels, slightly opposed blue-shift of around 9 cm^{-1} and red-shift of approximately 8 cm^{-1} happened on the D and G peaks, respectively, indicating the perturbation in the electronic state of GO due to the presence of OapPOSS. The ratio of the intensity of I_D to I_G bands was employed to evaluate the disorderliness of specimens [45, 52, 53]. The intensity ratio of the I_D/I_G band in GOPOS aerogels (1.01 for GOPOS90 and 1.07 for GOPOS10) faintly upraised, compared to pristine GO (0.96). This is a further indication of declining dimension of the in-plane sp^2 carbon atom domains and slightly disordered crystal arrangement of the GO platelets, induced by the bulky OapPOSS cages [44].

Shortly, OapPOSS molecules intercalate between layers of GO, lead to lattice expansion of GO and a disorder of the sp^2 carbon domains in the GO. These observations match well with the XRD patterns, coming next.

Lattice spacing structure of synthesized GOPOS aerogels

The X-Ray Diffraction (XRD) patterns of raw materials, intermediate, and typically GOPOS10 and GOPOS90 final aerogel samples, as shown in Fig. 6, were studied to find out more clues for the expansion of GO lattice caused by the OapPOSS intercalation.

Sharp and single characteristic peak of graphene can be effortlessly discerned at 2θ=26.5°. As expected, this equivalent band for GO was transferred to lower diffraction angle, 2θ =11.2°, representing interlayer spacing upon oxidation of graphene. In the XRD pattern of OapPOSS two diffraction peaks were found; a sharp one

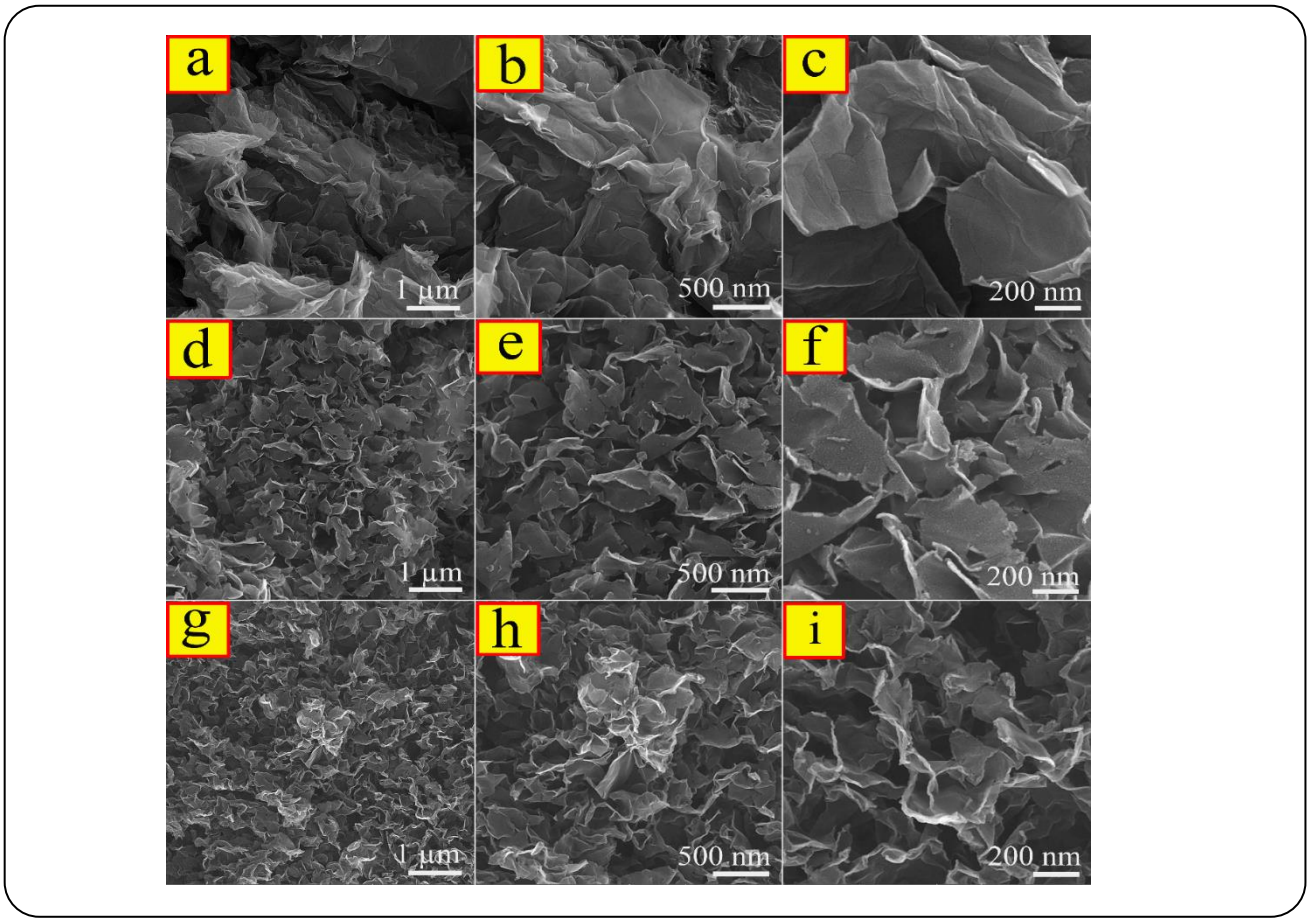

Fig. 7: FESEM micrographs of typical samples: GO (a-c), GOPOS10 aerogel (d-f), and GOPOS90 aerogel (g-i) with different magnifications (35.0 kx, 75.0 kx, 150 kx).

at about 2θ=8.1° and another widespread one at 2θ=15° to 31°, demonstrating the worse crystallinity structure caused by a dissimilar situation of amino groups introduced into each phenyl [42, 52]. In XRD pattern of all GOPOS aerogels, characteristic diffraction bands of pristine materials were entirely disappeared and presented no And from another point of view, OapPOSS moieties are well dispersed upon the reaction. According to the Fig. 6, fully lattice expansion can be achieved even in the small amount of OapPOSS molecules.

The microstructure of GOPOS aerogels

To study the microstructure of the GOPOS aerogels the Field Emission Scanning Electron Microscopy (FESEM) images under various magnifications are introduced in Fig. 7.

According to the micrographs, the network arrangement and great interstitial pore can be detected diffraction peak. This illustrates, from one point of view, that the covalently attached OapPOSS molecules cause an intensified lattice expansion of GO nanosheets in the GOPOS aerogels leading to completely a disordered GO structure.

in all GOPOS aerogels. In fact, a definite, linked-together 3D porous network and a randomly oriented 3D framework of pore walls, which established of slim platelets of the stacked assembly of GO, can be explicitly perceived. The pore size of the scaffold is in between nanoscale to several microns. All GOPOS aerogels were clearly made of multiple assemblies of GO nanosheets in the form of fractals and remain unaffected in magnitude in all compositions. GO platelets seem smooth, with folds and wrinkling in the FESEM micrographs of all GOPOS aerogels. As can be observed from the micrograph images of typically GOPOS10, presented in Fig. 7d-f and

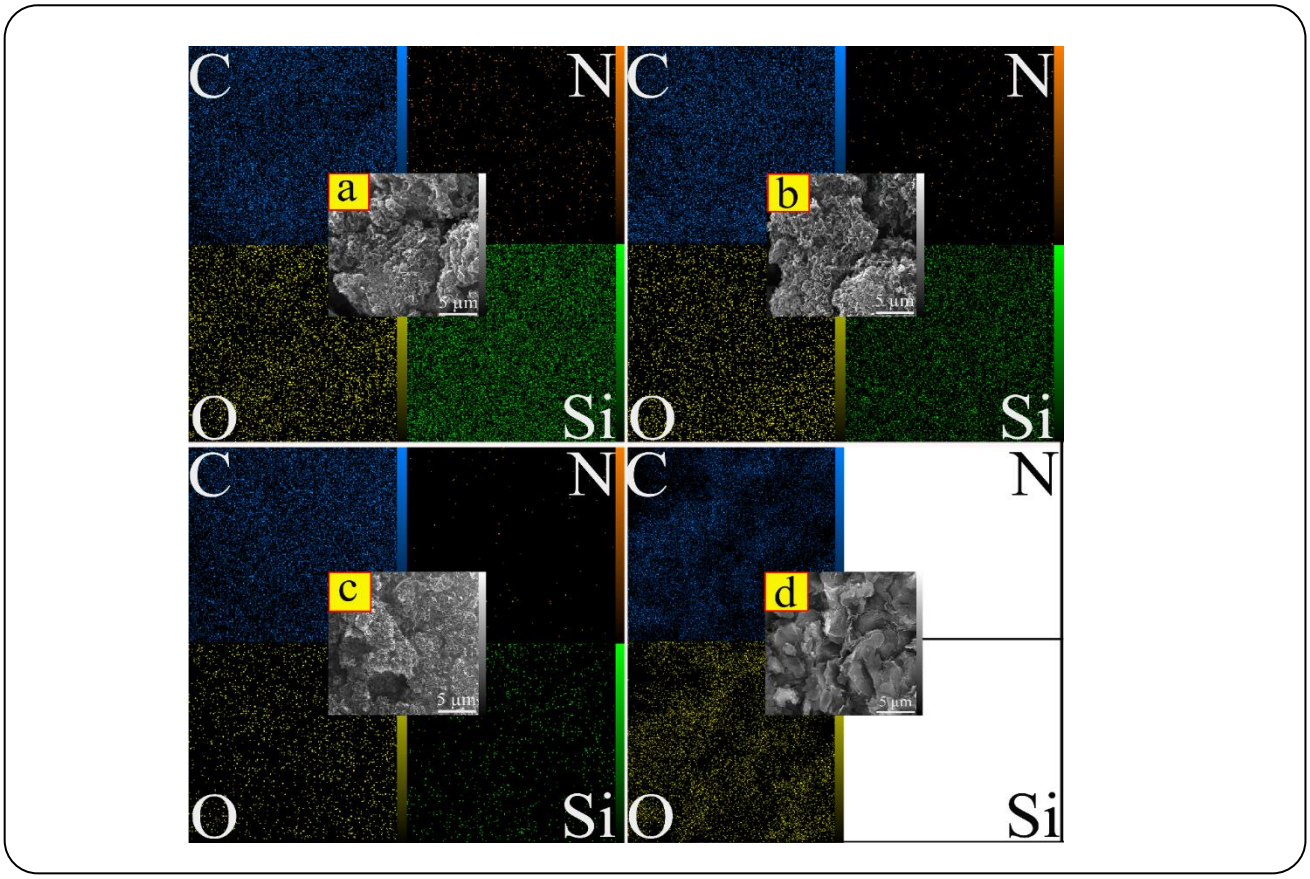

Fig. 8: EDS elemental mapping and FE-SEM images (center) of the GOPOS10 (a), GOPOS50 (b), GOPOS90 (c), and GO (d).

GOPOS90, demonstrated in Fig. 7g-i, OapPOSS moieties were uniformly distributed on GO platelets with no obvious aggregation even at high concentration and high resolution (supporting Figs. S6 and S7) [29, 54].

To visualize the elemental distribution and quantification of the presented elements in the internal microstructure of GOPOS specimens, the Energy Dispersive X-ray Spectrometry (EDS)-elemental mapping images were employed (Fig. 8).

As can be understood from the mapping images of typically GOPOS10, GOPOS50, and GOPOS90 presented in Fig. 8a-c, the silicone and nitrogen atoms of OapPOSS molecules were emitted uniformly in the EDS mapping of the equivalent FESEM section of all specimens. It can be deduced that OapPOSS nanoparticles were almost evenly distributed on the surfaces of GO platelets with no aggregation. Pristine GO, displayed in Fig. 8d, merely introduced the carbon and oxygen elements, which derive from GO. With further OapPOSS concentration, the sharp intensity level of Si and N atoms signals is detected, revealing more OapPOSS molecules has been successfully incorporated onto the GO nanosheets. Further information regarding EDS elemental mapping are available in supporting Fig. S8. Furthermore, quantitative EDS X-ray results of FESEM micrographs of all samples are shown in Fig. 9.

Multi-point Brunauer-Emmett-Teller (BET) using nitrogen adsorption-desorption graphs of aerogels, demonstrated in Fig. 10, were engaged to distinguish the porous characteristics of the resultant aerogels.

A type IV isotherm with a clear hysteresis loop of capillary condensation at a wide P/P_0 extent of 0.29-1.0 was discovered, inferring the formation of triple hierarchical micro- meso- and macroporous structures in the skeletal framework. The emergence of the hysteresis loop at isotherms is a sign of the presence of mesoporous structures in the aerogel specimens [25, 54-57].

According to the calculated data acquired from the adsorption-desorption isotherms of BET-technique, the surface area of GOPOS aerogel samples is in the range of

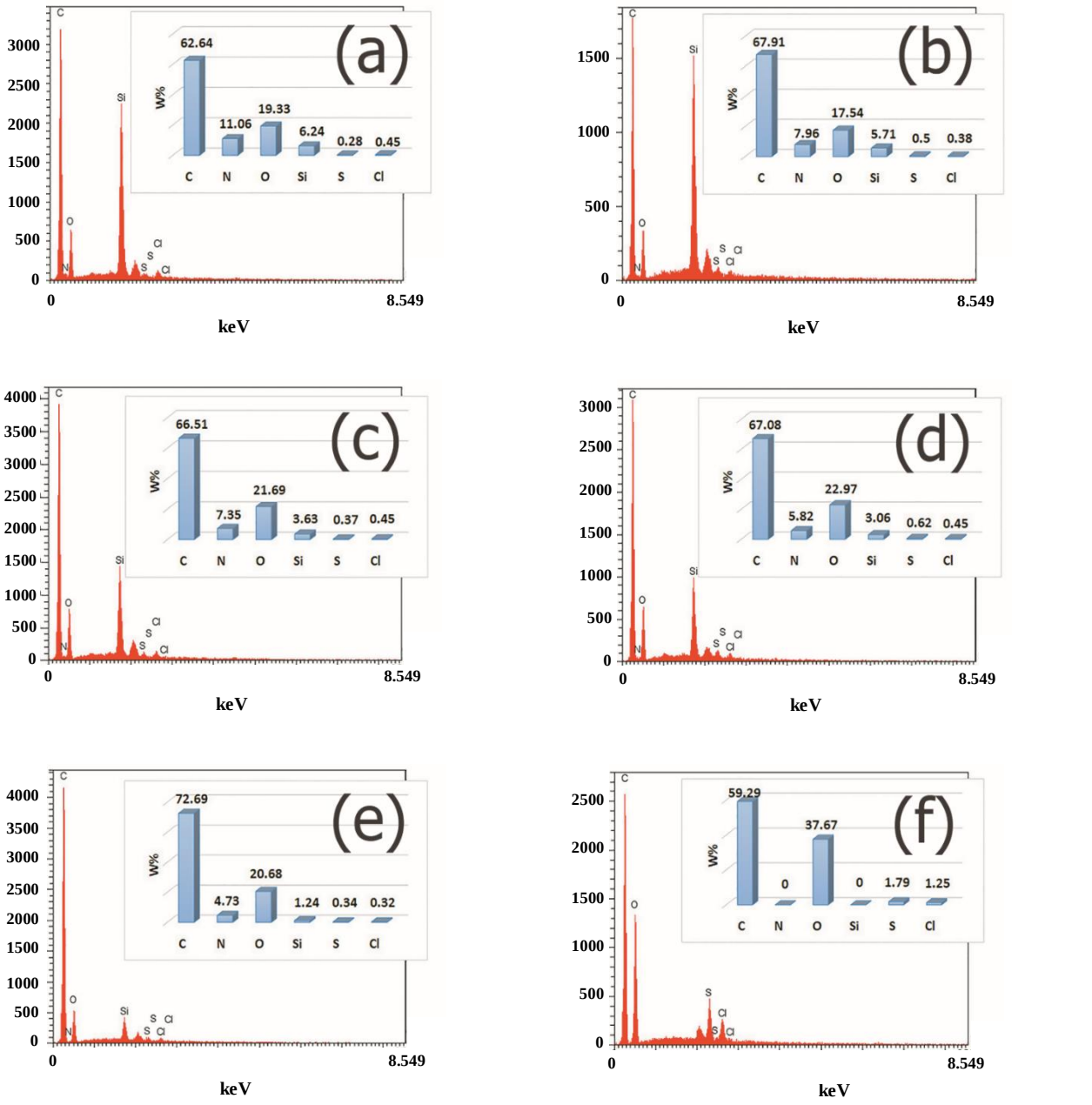

Fig. 9: Quantitative EDS X-ray results of FESEM micrographs of GOPOS10 (a), GOPOS30 (b), GOPOS50 (c), GOPOS70 (d), GOPOS90 (e), and GO (f).

250 to 713 m^2/g. As well, average pore diameter, D_{pore}, (obtained from Barrett-Joiner-Halenda, BJH) and total pore volume, V_{pore}, of the aerogels, fall between 18 to 42 nm and 2.6 to 4.0 cm^3/g, respectively (Table 2).

However, macro-pore cavities (the pores greater than 50 nm) are not detected by N_2 sorption technique. The value of D_{pore} and V_{pore} of the aerogels were calculated by equation 1 and 2 (Table 2) [58].

$$\text{Average pore diameter, } D_{pore},(\text{nm}) = \frac{4 \times \text{pore volume}}{S_{BET}} \quad (1)$$

$$\text{Total pore volume, } V_{pore},\left(\text{cm}^3\ \text{g}^{-1}\right) = \frac{1}{\rho_b} - \frac{1}{\rho_s} \quad (2)$$

As already mentioned, OapPOSS nanoparticles uniformly decorate the entire surface of the GO platelets and may even occupy the micro-scale pores [56].

Table 2: Morphological characteristics and pore size of GOPOS aerogel samples.

Sample	GOPOS10	GOPOS30	GOPOS50	GOPOS70	GOPOS90
ρ_s [g cm^{-3}] ± 0.1	1.56	1.61	1.72	1.85	1.98
ρ_b [mg cm^{-3}] ± 0.1[a)]	2.7	3.4	4.5	5.2	5.9
Porosity [%][b)]	> 99.5	> 99.5	> 99.5	> 99.5	> 99.5
V_{micro} [cm^3 g^{-1}]	0.07	0.16	0.18	0.23	0.27
V_{meso} [cm^3 g^{-1}]	0.69	1.55	1.73	2.03	2.31
V_{pore} calculated by equation 2 [cm^3 g^{-1}]	370	293	222	192	169
D_{pore} calculated by equation 1 [µm]	5.92	1.90	1.35	1.11	0.9
Surface area [m^2 g^{-1}]	250	624	656	687	713
Shrinkage during gelation [%]	42	38	31	27	19
Physical form	monolith	monolith	monolith	monolith	monolith
Strength	poor	poor	fair	good	good

a) ((The bulk density of the aerogels, calculated by $\rho_b = m_s/V_s$, by dividing the weight (m_s) to the specimen volume (V_s))); b) ((Porosity percent calculated by $\left(1 - \frac{\rho_b}{\rho_s}\right) \times 100$)).

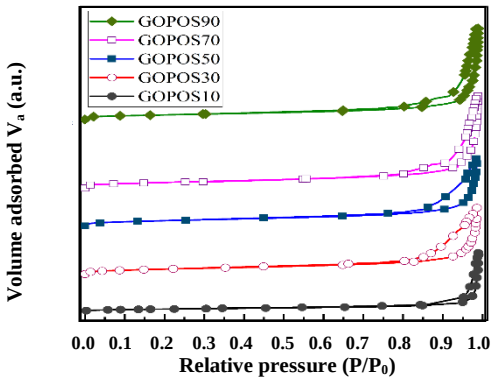

Fig. 10: N2 adsorption-desorption isotherms of the GOPOS aerogels.

Therefore, as a general trend, the minor OapPOSS content result in the less occupied and consequently the major available micro- and mesoporous, leading to the greater surface area, as well as greater micro- and mesopore volume.

Similarly, the pore size distribution graph extracted from the desorption branch by means of the BJH technique disclosed that only a single peak for all aerogels, suggesting OapPOSS nanoparticles are decorated and distributed almost smoothly and uniformly on the surface of GO nanosheets, approving the EDS elemental spectrum and FESEM images.

In accordance with BET results (Table 2), and as can be realized from SEM images (Fig. 7d-i), GOPOS90 sample, possessing the lower value of OapPOSS, has got more micro- and mesopores and fewer macropores leading to the higher specific surface area.

The bulk density of the aerogel samples was located between the super low values of 2.7 to 5.9 mg cm^{-3}. As the collected data are shown in Table 2, the lower GO content leads to the lower skeletal density and bulk density. The porosity of all aerogel samples was beyond the value of 99.5 %.

CONCLUSIONS

A conspicuous synthetic approach to preparing high porous and ultra-flyweight GOPOS hybrid aerogels, comprising different contents of OapPOSS, was established. The GOPOS hybrid aerogels were successfully fabricated by a solution-based self-assembly procedure, followed by solvent exchange and CO_2 supercritical drying, using GO as the backbone of aerogels and OapPOSS as the structural enhancer. It was verified that OapPOSS-containing graphene aerogels were synthesized by covalent interaction of OapPOSS and GO. The pieces of evidence obtained from XRD patterns clarified that the OapPOSS increase the lattice expansion of GO, leading to fully disorder the structure of GO. Results obtained from FESEM micrographs revealed that

there are a definite linked-together 3D porous network and a randomly oriented 3D framework of pore walls of the assembly of stacked GO nanosheets. Based on EDS mapping, the severe intensity level of Si and N atoms signals, illuminating more OapPOSS molecules have been successfully hosted onto the GO nanoplatelets. A type IV nitrogen adsorption/desorption isotherm with a hysteresis loop in a wide P/P_0 extent of 0.29 - 1.0 were observed indicating the formation of triple hierarchical micro- meso- and macroporous structures in the skeletal frameworks. Skeletal density and bulk density of aerogels were placed between 1.56 to 1.98 g cm^{-3} and super-low values of 2.7 to 5.9 mg cm^{-3}, respectively. The above-mentioned remarkable properties of obtained aerogels, develop their potential application in thermal insulation/ protection, oil absorption, energy storage, and preparation of catalyst supports and supercapacitors. Thermal stability, thermal conductivity, electrical and mechanical properties of these GOPOS aerogels will be reported in the future.

SUPPLEMENTARY MATERIALS AVAILABLE

Materials such as FT-IR, UV/Vis, high magnification of FESEM micrographs, and EDS elemental mapping of synthesized aerogels, and digital photos during all stages of the aerogel preparation process are available from the Iranian Journal of Chemistry and Chemical Engineering (IJCCE) Online publications website or the author.

Acknowledgments

We would like to express our special and immense appreciation to Mr. Mahmood Akbari Baseri for his encouragement throughout this research.

Received : Jul. 10, 2019 ; Accepted : Jan. 13, 2020

REFERENCES

[1] Boehm H.-P., Graphene—How a Laboratory Curiosity Suddenly Became Extremely Interesting, *Angewandte Chemie International Edition*, **49(49)**: 9332-9335 (2010).

[2] Lee C., Wei X., Kysar J.W., Hone J., Measurement of the Elastic Properties and Intrinsic Strength of Monolayer Graphene, *Science*, **321(5887)**: 385-388 (2008).

[3] Orlita M., Faugeras C., Plochocka P., Neugebauer P., Martinez G., Maude D.K., Barra A.L., Sprinkle M., Berger C., de Heer W.A., Potemski M., Approaching the Dirac Point in High-Mobility Multilayer Epitaxial Graphene, *Physical Review Letters*, **101(26)**: 267601 (2008).

[4] Balandin A.A., Ghosh S., Bao W., Calizo I., Teweldebrhan D., Miao F., Lau C.N., Superior Thermal Conductivity of Single-Layer Graphene, *Nano Letters*, **8(3)**: 902-907 (2008).

[5] Park S., Ruoff R.S., Chemical Methods for the Production of Graphenes, *Nature Nanotechnology*, **4**: 217-224 (2009).

[6] Chen D., Feng H., Li J., Graphene oxide: Preparation, Functionalization, and Electrochemical Applications, *Chemical Revie*ws, **112(11)**: 6027-6053 (2012).

[7] Zhu C., Han T. Y.-J., Duoss E. B., Golobic A. M., Kuntz J. D., Spadaccini C. M., Worsley M. A., Highly Compressible 3d Periodic Graphene Aerogel Microlattices, *Nature Communications*, **6**: 6962 (2015).

[8] Xue Y., Wu B., Bao Q., Liu Y., Controllable Synthesis Of Doped Graphene And Its Applications, *Small*, **10(15)**: 2975-2991 (2014).

[9] Xu Y., Liu J., Graphene as Transparent Electrodes: Fabrication and New Emerging Applications, *Small*, **12(11)**: 1400-1419 (2016).

[10] Sun H., Xu Z., Gao C., Multifunctional, Ultra-Flyweight, Synergistically Assembled Carbon Aerogels, *Advanced Materials*, **25(18)**: 2554-2560 (2013).

[11] Nardecchia S., Carriazo D., Ferrer M. L., Gutierrez M. C., del Monte F., Three Dimensional Macroporous Architectures and Aerogels Built of Carbon Nanotubes and/or Graphene: Synthesis and Applications, *Chemical Society R*eviews, **42(2)**: 794-830 (2013).

[12] Mao J., Iocozzia J., Huang J., Meng K., Lai Y., Lin Z., Graphene Aerogels For Efficient Energy Storage and Conversion, *Energy & Environmental Science*, **11(4)**: 772-799 (2018).

[13] Wang H., Feng H., Li J., Graphene and Graphene-Like Layered Transition Metal Dichalcogenides in Energy Conversion and Storage, *Small*, **10(11)**: 2165-2181 (2014).

[14] Yang M., Jeong J.-M., Huh Y. S., Choi B. G., High-Performance Supercapacitor Based on Three-Dimensional MoS_2/Graphene Aerogel Composites, *Composites Science and Technology*, **121**: 123-128 (2015).

[15] Yu H., Xin G., Ge X., Bulin C., Li R., Xing R., Zhang B., Porous Graphene-Polyaniline Nanoarrays Composite with Enhanced Interface Bonding and Electrochemical Performance, *Composites Science and Technology*, **154**: 76-84 (2018).

[16] Pottathara Y. B., Bobnar V., Finšgar M., Grohens Y., Thomas S., Kokol V., Cellulose Nanofibrils-Reduced Graphene Oxide Xerogels And Cryogels for Dielectric and Electrochemical Storage Applications, *Polymer*, **147**: 260-270 (2018).

[17] He C., Qiu S., Peng H., Zhang Q., Han X., Yang Y., Shi D., Xie X., Combination of 1d ni(oh)2 Nanobelts ad 2d Graphene Sheets to Fabricate 3d Composite Hydrogel Electrodes with Ultrahigh Capacitance and Superior Rate Capability, *Composites Science and Technology*, **167**: 155-163 (2018).

[18] Zhang X., Sui Z., Xu B., Yue S., Luo Y., Zhan W., Liu B., Mechanically Strong and Highly Conductive Graphene Aerogel and Its Use as Electrodes for Electrochemical Power Sources, *Journal of Materials Chemistry*, **21(18)**: 6494-6497 (2011).

[19] Wu H., Wang Z.-M., Kumagai A., Endo T., Amphiphilic Cellulose Nanofiber-Interwoven Graphene Aerogel Monolith for Dyes and Silicon Oil Removal, *Composites Science and Technology*, **171**: 190-198 (2019).

[20] Zhu L., Wang Y., Wang Y., You L., Shen X., Li S., An environmentally Friendly Carbon Aerogels Derived from Waste Pomelo Peels for the Removal of Organic Pollutants/Oils, *Microporous and Mesoporous Materials*, **241**: 285-292 (2017).

[21] Szczęśniak B., Choma J., Jaroniec M., Effect of Graphene Oxide on the Adsorption Properties of Ordered Mesoporous Carbons Toward H_2, C_6H_6, CH_4 and CO_2, *Microporous and Mesoporous Materials*, **261**: 105-110 (2018).

[22] Li H., Fan J., Shi Z., Lian M., Tian M., Yin J., Preparation and Characterization of Sulfonated Graphene-Enhanced Poly (Vinyl Alcohol) Composite Hydrogel and its Application as Dye Absorbent, *Polymer*, **60**: 96-106 (2015).

[23] Raeisi N., Salman Tabrizi N., Sangpour P., Synthesis of Sodium Alginate-Derived Carbon Aerogel for Adsorptive Removal of Methylene Blue, *Iranian Journal of Chemistry and Chemical Engineering (IJCCE)*, **39(5)**: 157-168 (2020).

[24] Moghaddas J., Amirkhani L., Jafarizadeh H., Optimization of Biodiesel Production Using Immobilized Candida Rugosa Lipase on Magnetic Fe_3O_4-Silica Aerogel, *Iranian Journal of Chemistry and Chemical Engineering (IJCCE)*, **38(2)**: 193-201 (2019).

[25] Worsley M. A., Pham T. T., Yan A., Shin S. J., Lee J. R. I., Bagge-Hansen M., Mickelson W., Zettl A., Synthesis and Characterization of Highly Crystalline Graphene Aerogels, *ACS Nano*, **8(10)**: 11013-11022 (2014).

[26] Sun F., Yang J., Zhang H., Yi L., Luo K., Zhao L., Wu J., Multi-Functional Composite Aerogels Enabled By Chemical Integration of Graphene Oxide and Waterborne Polyurethane Via a Facile and Green Method, *Composites Science and Technology*, **165**: 175-182 (2018).

[27] Yue C., Feng J., Feng J., Jiang Y., Thermal Conductivity of Aerogel Composites with Oriented Nitrogen-Doped Graphene, *Composites Science and Technology*, **146**: 198-202 (2017).

[28] Paredes J. I., Villar-Rodil S., Martínez-Alonso A., Tascón J. M. D., Graphene Oxide Dispersions in Organic Solvents, *Langmuir*, **24(19)**: 10560-10564 (2008).

[29] Whitby R. L. D., Chemical Control of Graphene Architecture: Tailoring Shape and Properties, *ACS Nano*, **8(10)**: 9733-9754 (2014).

[30] Chen W., Yan L., In Situ Self-Assembly of Mild Chemical Reduction Graphene for Three-Dimensional Architectures, *Nanoscale*, **3(8)**: 3132-3137 (2011).

[31] Compton Owen C., Nguyen SonBinh T., Graphene Oxide, Highly Reduced Graphene Oxide, and Graphene: Versatile Building Blocks for Carbon-Based Materials, *Small*, **6(6)**: 711-723 (2010).

[32] Fan L., Li X., Song X., Hu N., Xiong D., Koo A., Sun X., Promising Dual-Doped Graphene Aerogel/SnS2 Nanocrystal Building High-Performance Sodium-Ion Batteries, *ACS Applied Materials & Interfaces*, **10(3)**: 2637-2648 (2018).

[33] Benzigar M. R., Talapaneni S. N., Joseph S., Ramadass K., Singh G., Scaranto J., Ravon U., Al-Bahily K., Vinu A., Recent Advances in Functionalized Micro and Mesoporous Carbon Materials: Synthesis and Applications, *Chemical Society Reviews*, **47(8)**: 2680-2721 (2018).

[34] Qiu B., Xing M., Zhang J., Recent Advances in Three-Dimensional Graphene-Based Materials for Catalysis Applications, *Chemical Society Reviews*, **47(6)**: 2165-2216 (2018).

[35] Alhwaige A. A., Herbert M. M., Alhassan S. M., Ishida H., Qutubuddin S., Schiraldi D. A., Laponite/Multigraphene Hybrid-Reinforced Poly(Vinyl Alcohol) Aerogels, *Polymer*, **91**: 180-186 (2016).

[36] Qiu B., Xing M., Zhang J., Mesoporous TiO_2 Nanocrystals Grown in Situ on Graphene Aerogels for High Photocatalysis and Lithium-Ion Batteries, *Journal of the American Chemical Society*, **136(16)**: 5852-5855 (2014).

[37] Hosseini H., Kokabi M., Mousavi S. M., BC/rGO Conductive Nanocomposite Aerogel as a Strain Sensor, *Polymer*, **137**: 82-96 (2018).

[38] Joshi M., Butola B. S., Polymeric Nanocomposites—Polyhedral Oligomeric Silsesquioxanes (Poss) as Hybrid Nanofiller, *Journal of Macromolecular Science, Part C*, **44(4)**: 389-410 (2004).

[39] Phillips S. H., Haddad T. S., Tomczak S. J., Developments in Nanoscience: Polyhedral Oligomeric Silsesquioxane (poss)-Polymers, *Current Opinion in Solid State and Materials Science*, **8(1)**: 21-29 (2004).

[40] Zhou H., Ye Q., Xu J., Polyhedral oligomeric silsesquioxane-based hybrid materials and their applications, *Materials Chemistry Frontiers*, **1(2)**: 212-230 (2017).

[41] Pielichowski K., Njuguna J., Janowski B., Pielichowski J., Polyhedral Oligomeric Silsesquioxanes (poss)-Containing Nanohybrid Polymers, *Supramolecular Polymers Polymeric Betains Oligomers*, Springer Berlin Heidelberg, Berlin, Heidelberg, 225-296 (2006).

[42] Liao W.-H., Yang S.-Y., Hsiao S.-T., Wang Y.-S., Li S.-M., Ma C.-C. M., Tien H.-W., Zeng S.-J., Effect of Octa(aminophenyl) Polyhedral Oligomeric Silsesquioxane Functionalized Graphene Oxide on the Mechanical and Dielectric Properties of Polyimide Composites, *ACS Applied Materials & Interfaces*, **6(18)**:15802-15812 (2014).

[43] Hu L., Jiang P., Bian G., Huang M., Haryono A., Zhang P., Bao Y., Xia J., Effect of Octa(aminopropyl) Polyhedral Oligomeric Silsesquioxane (Oapposs) Functionalized Graphene Oxide on the Mechanical, Thermal, and Hydrophobic Properties of Waterborne Polyurethane Composites, *Journal of Applied Polymer Science*, **134(6)**: 44440 (2016).

[44] Xue Y., Liu Y., Lu F., Qu J., Chen H., Dai L., Functionalization of Graphene Oxide with Polyhedral Oligomeric Silsesquioxane (Poss) for Multifunctional Applications, *The Journal of Physical Chemistry Letters*, **3(12)**: 1607-1612 (2012).

[45] Zong P., Fu J., Chen L., Yin J., Dong X., Yuan S., Shi L., Deng W., Effect of Aminopropylisobutyl Polyhedral Oligomeric Silsesquioxane Functionalized Graphene on the Thermal Conductivity and Electrical Insulation Properties of Epoxy Composites, *RSC Advances*, **6(13)**:10498-10506 (2016).

[46] Namvari M., Du L., Stadler F. J., Graphene Oxide-Based Silsesquioxane-Crosslinked Networks - Synthesis and Rheological Behavior, *RSC Advances*, **7(35)**: 21531-21540 (2017).

[47] Xu Y., Sheng K., Li C., Shi G., Self-Assembled Graphene Hydrogel Via a One-Step Hydrothermal process, *ACS Nano*, **4(7)**: 4324-4330 (2010).

[48] Ou J., Wang J., Liu S., Mu B., Ren J., Wang H., Yang S., Tribology Study of Reduced Graphene Oxide Sheets on Silicon Substrate Synthesized Via Covalent Assembly, *Langmuir*, **26(20)**: 15830-15836 (2010).

[49] Yang H., Li F., Shan C., Han D., Zhang Q., Niu L., Ivaska A., Covalent Functionalization of Chemically Converted Graphene Sheets Via Silane and Its Reinforcement, *Journal of Materials Chemistry*, **19(26)**: 4632-4638 (2009).

[50] Wang X., Song L., Yang H., Xing W., Kandola B., Hu Y., Simultaneous Reduction and Surface Functionalization of Graphene Oxide with Poss for Reducing Fire Hazards In Epoxy Composites, *Journal of Materials Chemistry*, **22(41)**: 22037-22043 (2012)

[51] Dreyer D. R., Park S., Bielawski C. W., Ruoff R. S., The Chemistry of Graphene Oxide, *Chemical Society Reviews*, **39(1)**: 228-240 (2010).

[52] Yu W., Fu J., Dong X., Chen L., Shi L., A Graphene Hybrid Material Functionalized with Poss: Synthesis and Applications in Low-Dielectric Epoxy Composites, *Composites Science and Technology*, **92**: 112-119 (2014).

[53] Stankovich S., Dikin D. A., Piner R. D., Kohlhaas K. A., Kleinhammes A., Jia Y., Wu Y., Nguyen S. T., Ruoff R. S., Synthesis of Graphene-Based Nanosheets Via Chemical Reduction of Exfoliated Graphite Oxide, *Carbon*, **45(7)**: 1558-1565 (2007).

[54] Worsley M. A., Kucheyev S. O., Mason H. E., Merrill M. D., Mayer B. P., Lewicki J., Valdez C. A., Suss M. E., Stadermann M., Pauzauskie P. J., Satcher J. H., Biener J., Baumann T. F., Mechanically Robust 3D Graphene Macro Assembly with High Surface Area, *Chemical Communications*, **48(67)**: 8428-8430 (2012).

[55] Si W., Wu X., Zhou J., Guo F., Zhuo S., Cui H., Xing W., Reduced Graphene Oxide Aerogel with High-Rate Supercapacitive Performance in Aqueous Electrolytes, *Nanoscale Research Letters*, **8(1)**: 247 (2013).

[56] Duan Y., Fundamental Studies on Polymer and Organic-Inorganic Hybrid Nanoparticles Reinforced Silica Aerogels, Akron1333079860 (2012).

[57] Maleki H., Montes S., Hayati-Roodbari N., Putz F., Huesing N., Compressible, Thermally Insulating, and Fire Retardant Aerogels Through Self-Assembling Silk Fibroin Biopolymers Inside a Silica Structure-An Approach Towards 3D Printing of Aerogels, A*CS Applied Materials & Interfaces*, **10(26)**: 22718-22730 (2018).

[58] Maleki H., Durães L., Portugal A., Development of Mechanically Strong Ambient Pressure Dried Silica Aerogels with Optimized Properties, *The Journal of Physical Chemistry C*, **119(14)**: 7689-7703 (2015).